Advanced Steel Construction – Vol. 20 No. 1 (2024) 39–52
DOI:10.18057/IJASC.2024.20.1.5

COMPRESSION BEHAVIOUR OF BI-ANGLED BUILT-UP CRUCIFORMS LOADED THROUGH ONE ANGLE

Gorripotu Kishore Kumar * and Raghavan Ramalingam

Department of Civil Engineering, National Institute of Technology, Tiruchirappalli, India
** (Corresponding author: E-mail: gorripotukishorekumar@gmail.com)*

ABSTRACT

Angles are popularly used in built-up steel sections. The behaviour of common sections built-up by angles such as boxes and tees are established, and design provisions are available in design codes. The cruciform arrangement, consisting of vertex-to-vertex connected angles, has been studied recently as a strengthening arrangement for lattice tower primary members, where the load is not applied through the centroid on the built-up section, like in common built-up sections. The behaviour of such cruciforms need to be studied further for establishing their efficiency as compression members. This study consists of experimental tests followed by numerical parametric study of such cruciforms. Experimental tests on cruciform of slenderness 80, 100 and 120 were performed followed by numerical finite element analysis for validation. A parametric study was conducted on 36 bi-angled cruciforms with slenderness, connector spacing, number of bolts and angle width-thickness ratio as the chosen parameters. Predictions by national design codes were compared with the numerical results. The influence of these parameters on the load sharing rate between the angle sections were observed and it is seen that slenderness has the highest influence while the number of bolts per connector has least influence. Equal load sharing was achieved for cruciforms of lesser slenderness, showing that the arrangement can be an efficient strengthening arrangement.

ARTICLE HISTORY

Received: 21 June 2023
Revised: 9 October 2023
Accepted: 18 November 2023

KEYWORDS

Built-up section;
Cruciform;
Strengthening;
Compression

1. Introduction

Steel angles are the primarily used sections to construct lattice towers such as telecommunication and electrical transmission towers [1]–[3]. These towers are built by bolted connections of single or double angles for primary leg members and single angles for secondary members at higher elevation. Angles are also versatile due to which they are used in various built-up arrangements such as Tee (back to bank), Channel (toe to toe), box sections and design procedures for such built-up sections are available in international design standards. The behavior of angles is unique due to their unsymmetric geometry because of which Indian and other standards contain dedicated clauses to determine their compression capacity. Built-up sections in steel structures are adopted when the required cross-section to withstand the design load is not available and are recently also being adopted for retrofit of distressed members in service.

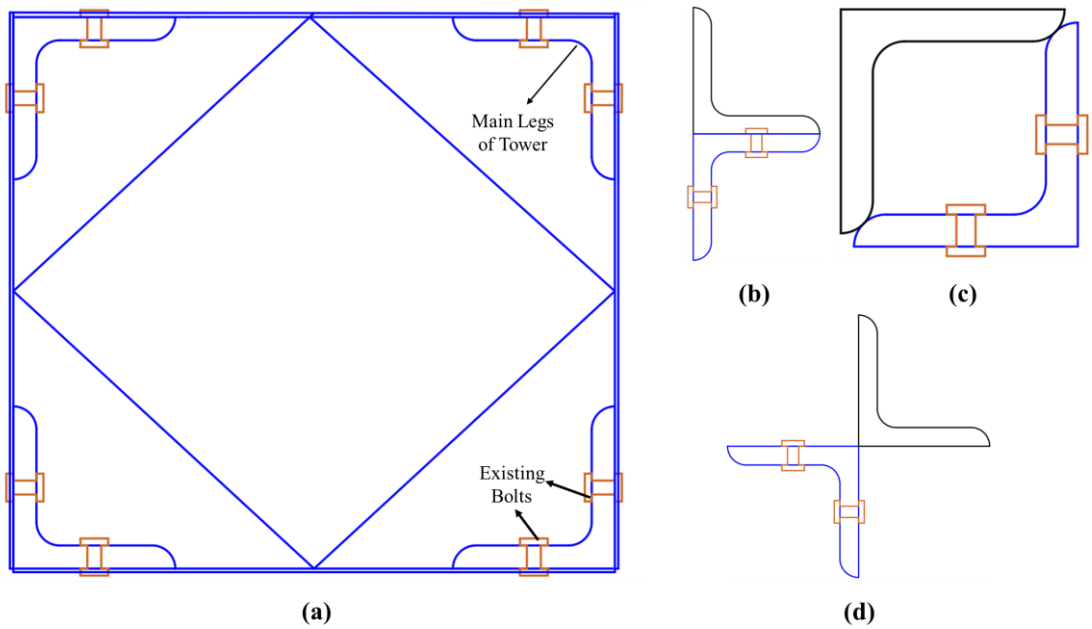

Fig. 1 Different Built-up options with angle sections for a tower; (a) Existence tower plan; (b) bi-angled T section; (c) bi-angled box section; (d) bi-angled cruciform section

Among various built-up options for existing tower legs for retrofit, Tee (Fig. 1 (b)) is not possible practically due to presence of bolts (Fig. 1 (a)) at both sides of the angle section and box section (Fig. 1(c)) is not possible due to presence of root radius at edges where the angles will have to be joined. Hence for an existing tower the cruciform arrangement offers the most practical solution since it minimally interferes with the two sides of the angle section which is to be retrofitted (Fig. 1(d)). A number of arrangements are cruciform by geometry (e.g., aligned, alternate etc.). But only the arrangement using uniformly spaced cleat angles for connecting the existing and reinforcing angles, have been called “cruciform” (Fig. 2) by researchers.

Extensive literature is available on the behaviour of built-up sections composed of angle sections. Tetra-angled cruciforms [4]–[6] have been studied as a built-up section comprising of angles as well as the effect of inter-connectors on the behaviour of these members. Flexural-Torsional buckling occurs depending on connector spacing [7] and overall slenderness [8]. Force sharing between the two members of a built-up section up to 30% have been seen in some studies [9], though this is influenced by the connection pattern viz. single cross plate, double cross plate, cleat angle etc.

Bolt-slip is a common occurrence in sections used in towers, with the most widely adopted slip model for the angle sections proposed by Ungkurapinan et. al [10] experimental programme. Recent studies demonstrate the resemblance

of joint models including slip [11] with experimental observation, and the initial torque has a prominent influence on ultimate load and stiffness [12]. The application of additional angles to strengthen towers is seen earlier in the form of diaphragm retrofit by Albermani [13], [14]. Among available tower primary leg retrofit patterns in literature, the studies by University of South Australia have determined that the cruciform is superior in terms of capacity improvement [15], and the improvement in tower ultimate capacity was also shown through testing of small-scale tower with leg-retrofit by cruciform arrangement [16]. Literature on efficiency of cruciform retrofit in improving the whole tower capacity are also present [17], [18]. Other retrofit options such as provision of casings [19], box [20] and others [21], [22] have also been attempted. Xie and Zhang [23] conducted an experimental test on a bottom panel of tower assembly by retrofitting the diagonal members and found that vulnerable members of the assembly changed from diagonal to main member after retrofitting. The component method of Eurocode 8 can be used to evaluate the connection in these members [24].

From the practical implementation view it is seen that the cruciform of Vertex-to-Vertex connection is more suitable [15], [22] for field application of retrofitting tower legs. But it is found that experimental work for determining in detail the behaviour of cruciform arrangement is lacking in the literature. Hence from the literature it is seen that further investigations on behaviour of cruciform of bi-angled section are needed to ascertain their effectiveness as a built-up section. Further, the existence-to-retrofit angle connections are to be specifically suitable for in-situ retrofitting. Such an option is presented in [15], [22]. The present study investigates the mechanical behavior of such cruciform retrofit section under compression loading experimentally and numerically using ABAQUS. Parameters chosen for study are (a) Slenderness Ratio, (b) Connector Spacing, (c) Number of bolts per connector and (d) Width to thickness ratio. The present study will help in understanding the ultimate behaviour of bi-angled cruciform section along with load sharing rate between Existing Member (EM) and newly added Reinforcing Member (RM).

2. Experimental setup

As shown in the Fig. 2 Vertex-to-vertex cleat angles were used to connect both Existing Member (EM) and Reinforcing Member (RM) to form the bi-angled Cruciform section with 5.6 grade of 10 mm sized bolt. Fig. 2 (a) and Fig. 2 (b) shows the cross-sectional views with connectors and without connectors, respectively. Fig. 2 (b) shows the loading point P and "e" is the eccentricity of the loading point, whereby load will be initially taken by EM then transferred to RM through Vertex-to-vertex cleat angles.

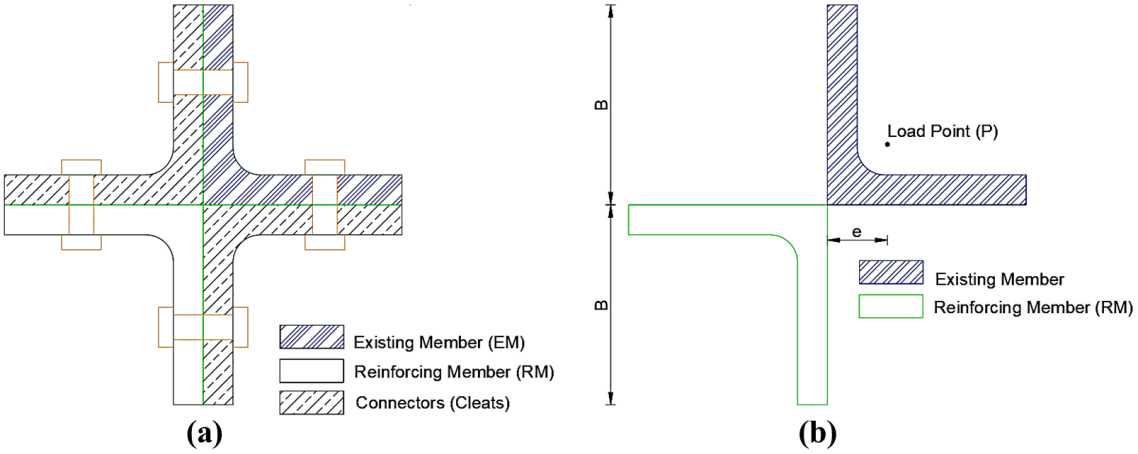

Fig. 2 Cross-sectional view of Bi-Angled Cruciform Section; (a) with connectors; (b) without connectors

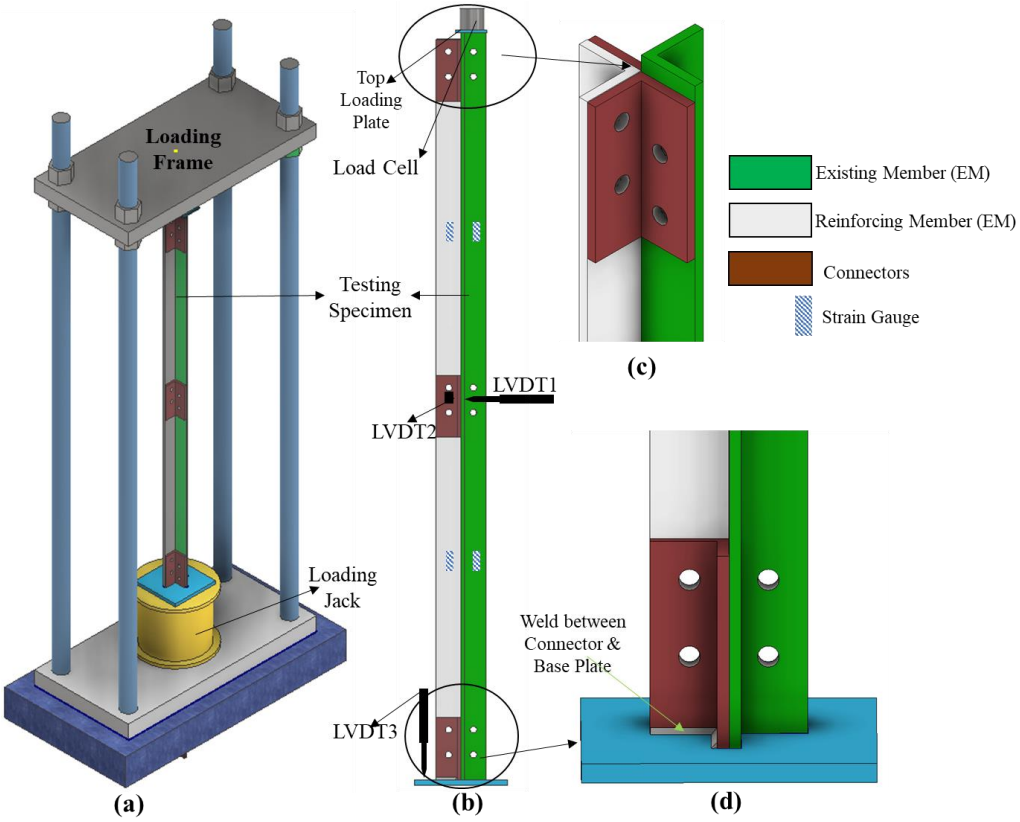

Fig. 3 Testing setup for Bi-Angled Cruciform Section with position of Strain gauge and LVDT

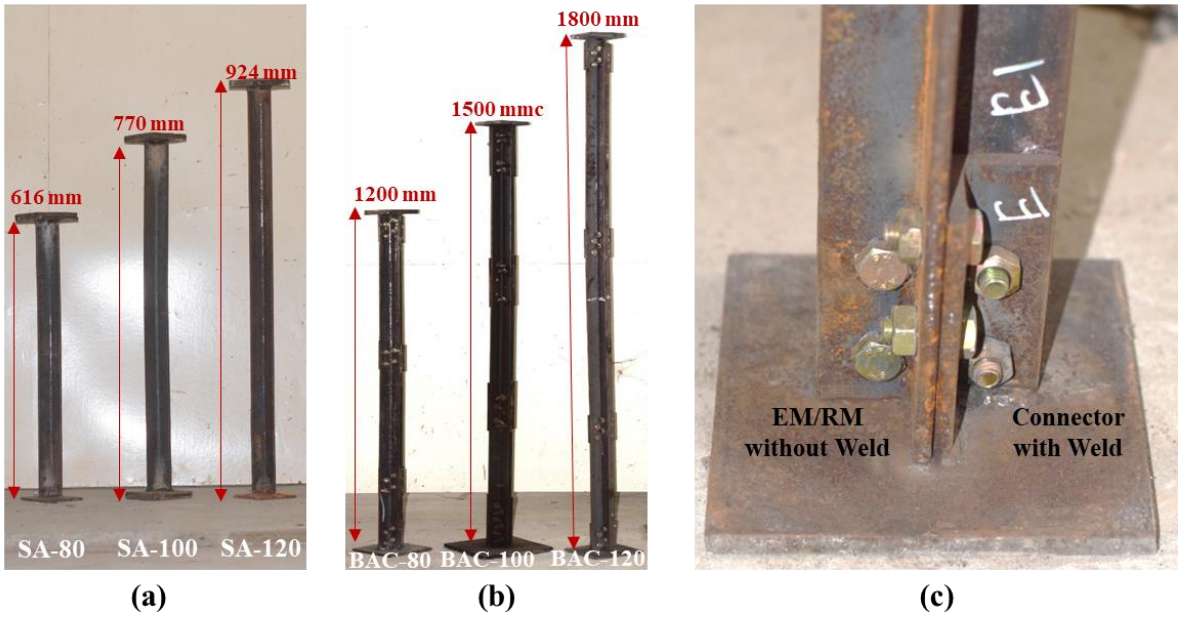

Fig. 4 Details of Experimental Specimens; (a) Single Angle specimens; (b) Bi-Angled Cruciform specimens; (c) Bottom Connector Details

The slenderness of the specimens of both single-angle and cruciform was chosen as the common parameter so that a comparative picture of change in failure (buckling) mode can be observed. The steel angle section of ISA 40X40X6 of E350 grade as per IS:2062-2011 was chosen for both single-angle and bi-angled cruciform experiments.

Fig. 3 mentions the detailed test setup and specimen details along with the location of strain gauges and LVDTs. A total of six strain gauges were used during the experiment for each Bi-Angled Cruciform (BAC) specimen, three for EM and three for RM. All these strain gauges were placed at the mid height of each segment (portion of specimen between two connectors). Three LVDTs (LVDT 1 and LVDT 2 to measure the lateral and transverse displacements at mid height and LVDT 3 to measure the axial displacement) were used. The loading point is the centroid of the EM (Fig. 2), and the top loading plate is welded only with EM (top of Fig. 3 (b)) . The level difference (Fig. 3 (c)) in the top surfaces of EM and RM, ensures that the load is initially taken by EM and then transferred to the RM through the bolted cleat angles over some distance.

The bottom plate was welded to the bottom connectors alone and not to the EM and RM (Fig. 3 (d) and Fig. 4 (c)). This was done in order to replicate the real field conditions where the main member of the tower is connected to the foundation via coping. During the experiment, some fabrication errors were found in the bi-angled cruciform section SR100 whereby the elevational difference between EM and RM was insufficient and SR120 specimen had an overall inclination of 2^0 with vertical. The same errors which occurred during fabrication were included in the numerical model later for model validation purpose.

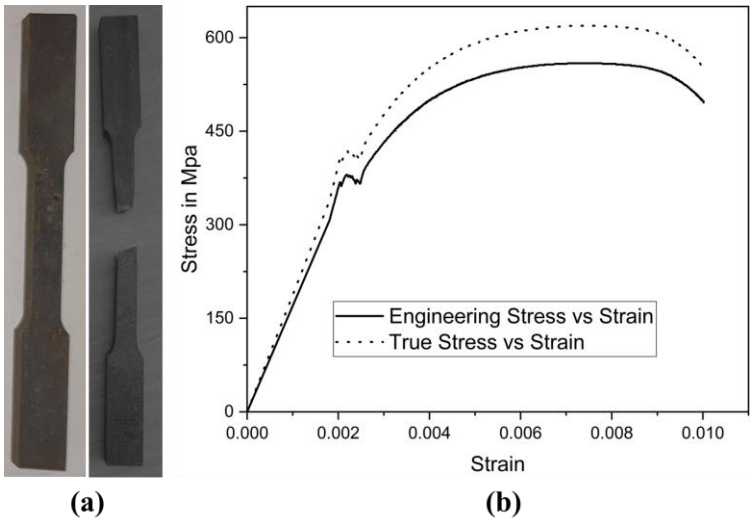

Fig. 5 Coupon Testing; (a) Coupon specimen before and after testing (b) Stress-Strain Plot

Eqn (1) to (5) were used to determine the various cross-sectional properties of BAC (Fig. 2 (b)), the chosen cruciform has cross-sectional area (A) 888 mm^2, centroidal moments of inertia (I_x) of both angles and product of inertia (I_{xy}) 260596 mm^4 and 56952 mm^4, respectively. The cleat angle are neglected for moment of inertia calculation of cruciform.

$$A = 2T\,(2B - T) \tag{1}$$

$$I_x = \frac{4B^4 - \{(B-T)^4 + 3(B^2 - T^2)\}}{6} \tag{2}$$

$$I_{xy} = \frac{T^2(2B^2 - T^2)}{2} \tag{3}$$

$$I_{min} = I_x - I_{xy} \tag{4}$$

$$r_{min} = \sqrt{\frac{I_{min}}{A}} \tag{5}$$

Bolt hole clearance, pitch, edge distance, and end distance are considered based on the regulations of IS:802-1995 (Code of Practice for structural steel Overhead Transmission Line Towers) [25] , while the centre-to-centre spacing of the connectors is based on the AISC 360-16 [26] specification, which states that individual components of compression members composed of two or more

shapes shall be connected to one another at intervals, *a*, such that the slenderness ratio, a/r_i, of each of the component shapes between the fasteners does not exceed three-fourths times the governing slenderness ratio of the built-up member. The least radius of gyration, r_i, shall be used in computing the slenderness ratio of each component part.

AISC 360-16 [26] suggests that for a built-up member to function as an effective structural member pretension is required. From the torque equation T=KFD, the required torque to obtain a pretension force of magnitude 10kN for bolts was evaluated as 20 N-m by considering K value as 0.2 [27] and this value of torque was applied to tighten the bolts. Sequence of tightening of bolts was performed from middle to outer as suggested in reference [10].

Three number of coupon specimens were extracted in accordance with the ASTM E8/E8M−13a [28] provisions and tension test was performed to find the grade of the steel and stress-strain properties. Fig. 5 (a) and Fig. 5 (b) shows the coupon specimen used for the tension test and average stress-strain (both engineering and true values) graph.

Detailed test setup for the single angles and cruciform specimens including location of LVDT, strain gauges, load cell shown in Fig. 3 The loading was stopped during each experiment after load started to drop, post the ultimate load based on safety considerations due to the deflection of specimen. Plots of load-deflection, strains and related results are plotted in section 4.

3. Numerical modelling

In order to obtain greater understanding on the physical behavior of these sections, a parametric study was performed. A numerical model was developed using ABAQUS. All parts named Existing Member (EM), Reinforcing Member (RM), and Connectors were created in the part module using the 3D solid extrude option. Bolt and nut were developed as a single unit called a fastener. The material density was taken as 7850 kg/m^3, with 0.3 as the friction coefficient. Boundary conditions of pinned at the base of bottom plate and twist and vertical deflection allowed at loading point were applied based on deformation observed in experiment.

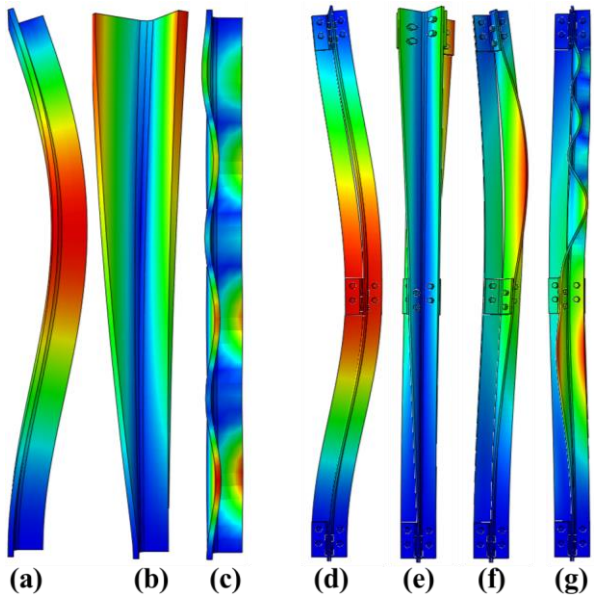

Fig. 6 Buckling Modes; (a) SA-F; (b) SA-T; (c) SA-LB; (d) BAC-F; (e) BAC-T; (f) BAC-FT; (g) BAC-LB

Table 1
List of models generated for Experimental results Validation and their global buckling modes

S. No	Name of Model	Size of Section	λ	L	First 4 Buckling Modes
1	SR80-SA-Num	ISA 40X40X6	80	616	F, T, LB, LB
2	SR100-SA-Num		100	770	F, T, LB, LB
3	SR120-SA-Num		120	924	F, T, LB, LB
4	SR80-BAC-Num		80	1200	F, T, TF, TF
5	SR100-BAC-Num		100	1500	F, T, TF, TF
6	SR100-BAC-Im-Num		100	1500	F, T, TF, TF
7	SR120-BAC-Num		120	1800	T, TF, F, TF
8	SR120-BAC-Im-Num		120	1800	T, TF, F, TF

SR, λ - Slenderness Ratio; L – Length of specimen; Num – Numerical model; Im – Imperfection modified; F - Flexural Buckling about Minor Axis; T - Torsional Buckling; TF - Torsional-

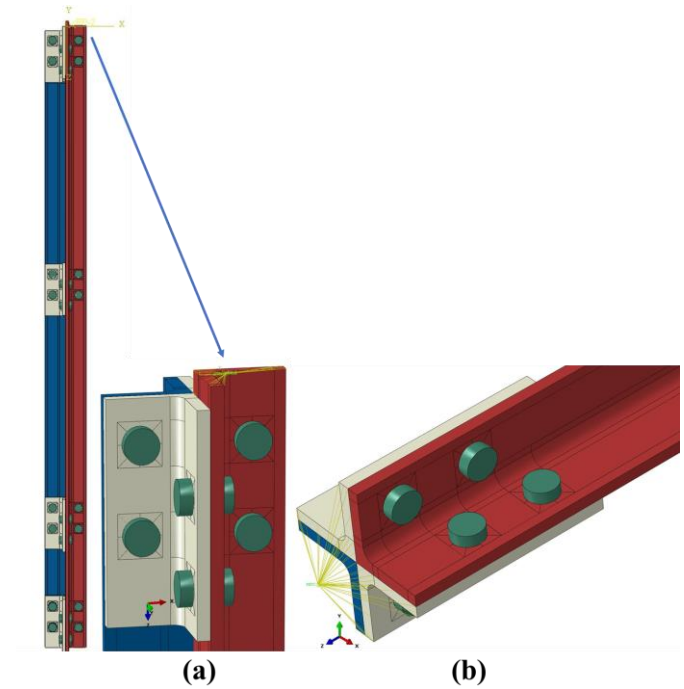

Fig. 7 Cruciform model with MPC connected to EM; (a) Top, (b) Bottom

Multipoint constraints (MPC) beam elements are used for application of boundary conditions and load (Fig. 7). The bolt load of 10kN is applied as the bolt pretension. The total analysis is conducted in two stages [3] – stage 1 includes the prediction of buckling modes from linear perturbation analysis to incorporate the imperfections. Stage 2 was non-linear analysis performed by Static-RIKS by incorporating the imperfections from stage 1 analysis. Imperfections factors of 0.5, 0.1, 0.1 and 0.1 (decided based on the trial and error to match with the experimental behaviour) for the first four buckling modes were incorporated through the keyword edit (Fig. 6, Table 1). Different global seed size of 5, 10 and 15 were tried for the analysis and it was found that ultimate behaviour was same for all mesh sizes and hence mesh size of 15 was adopted to minimize the computational time. Eight noded brick elements (C3D8R) with reduced integration were assigned [15], [29]. Two interactions were considered - penalty friction formulation with a friction coefficient of 0.25 in tangential behaviour and hard contacted pressure-overclosure with a penalty (Standard) for constraint enforcement method by specifying contact stiffness of 2000 N-mm with a linear behaviour [22].

4. Results and discussions

Experiments were performed on single angles and Bi-Angled cruciforms of same slenderness to evaluate their mechanical behaviour and capacities. Numerical validation of all models were done using the experimental results. Comparison of experiment and numerical results are presented in Table 2.

4.1. Experimental results

Table 2 shows the ultimate capacities obtained from testing. During the experiments, flexural buckling was observed for the all-single angles and cruciform sections of SR 80 and SR 100, whereas for SR 120 cruciform section, flexural-torsional buckling was observed. Due to insufficient elevational difference between EM and RM (SR 100 specimen) due to fabrication error, top plate attained contact with RM and therefore load was taken by both EM and RM from early stages of loading leading to higher failure load.

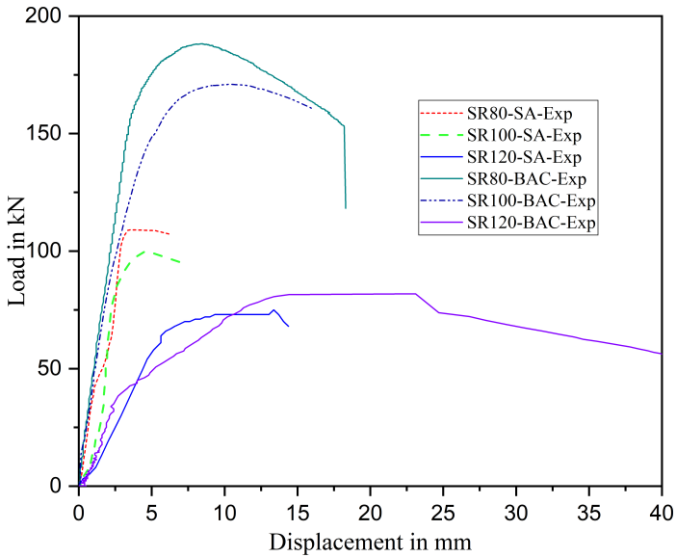

Fig. 8 Load vs Lateral Displacement for Single Angle (SA) and Bi-Angled Cruciform (BAC) Experiments

Fig. 8 show the load vs lateral displacement curves for all single angles and cruciform specimens, from the figure it is found that there is no much difference observed in the stiffness of both 80 and 100 slenderness specimens, whereas the stiffness of 120 slenderness specimen is significantly lower. This is because the Flexural-Torsional buckling drives the deflection of the specimen and also the effect of 2^0 inclination.

4.2. Numerical results and validation

For the specimen of slenderness 100 which had insufficient elevation difference between EM & RM, the ultimate capacity was 171.1kN since load was taken by both members from the start. Numerical capacity of SR100-BAC-Num was 169.26 kN. Therefore, a numerical model (SR100-BAC-Im-Num) of slenderness 100 was developed including the desired elevational difference between EM and RM and its capacity was 133.22 kN. Since SR120 model had an overall inclination of 2^0 the same was included in the numerical model for validation. The models 'SR120-BAC-Num' and 'SR120-BAC-Im-Num' are numerical models validated with inclination of 2^0 and without inclination, respectively.

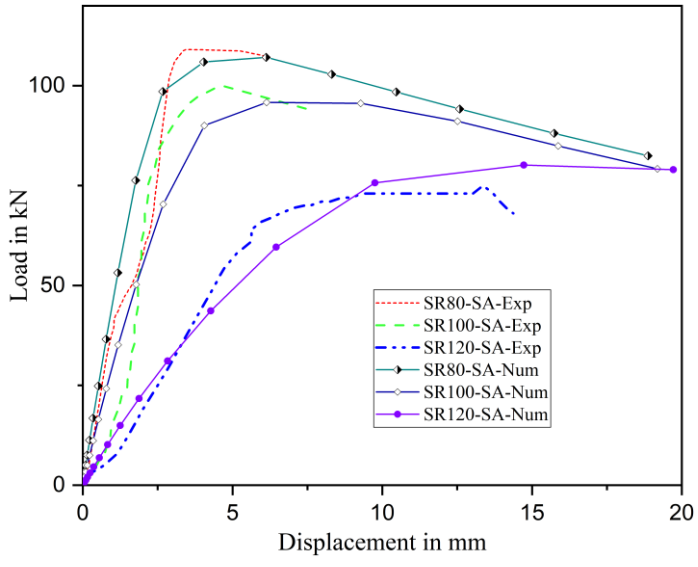

Fig. 9 Load vs Lateral Displacement for Single Angle Specimens

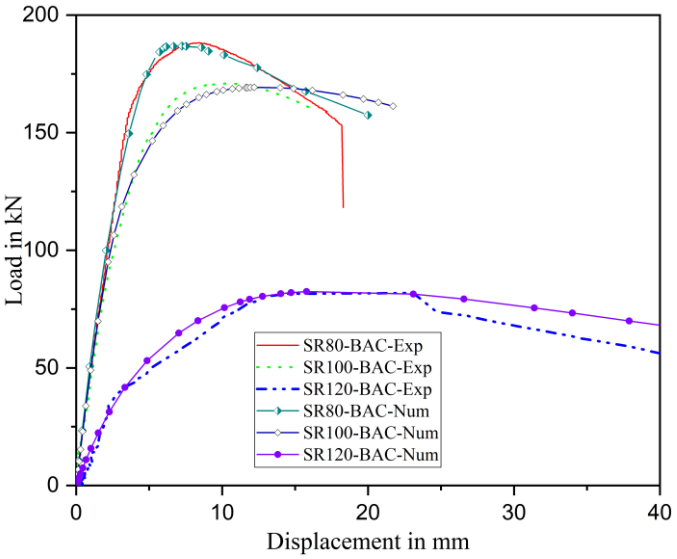

Fig. 10 Comparison of Exp-Num for Load vs Lateral Displacement for Bi -Angles Cruciform

For single angles and bi-angled Cruciform sections of all slenderness ratios, numerical capacity matched with experimental capacity and load vs lateral displacement curves (Fig. 9 and Fig. 10) were in good agreement with numerical results. The initial stiffness of SR80 and SR100 coincided and their load carrying capacities obtained from experiment (and numerical) were 188.2 kN (and 186.9 kN) and 171.1 kN (and 169.2 kN) respectively. The stiffness of 120 slenderness specimen is very low when compared with other slenderness specimens. Secondary moments in a column is prominent at higher slenderness ratios and also the eccentric loading amplifies the reduction in lateral stiffness in this specimen.

Comparison of load vs axial displacement for cruciform specimens are presented in Fig. 13. From that curves it is observed that, unlike lateral stiffness there is not much difference in axial stiffness between various slenderness specimens. As the curvature and the lateral deflection of a member increases, the compressive stresses on the concave side of the member also increases until the member fails due to excessive yielding. In the numerical analysis this corresponds to the increment where specimen reaches ultimate load. For Single angles (Fig. 11) and bi-angled Cruciform specimens (Fig. 12) the bending was observed about minor axis (v-v axis) in both experimental and numerical analysis.

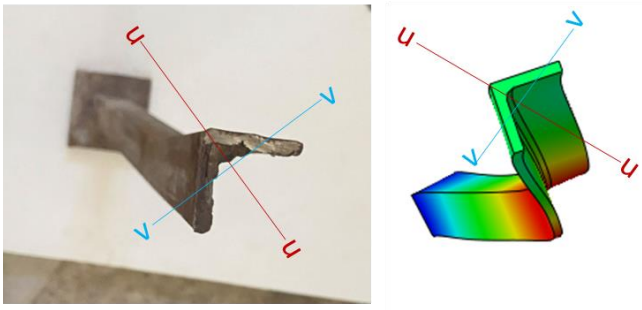

Fig. 11 Buckling axis for Single Angle Specimen

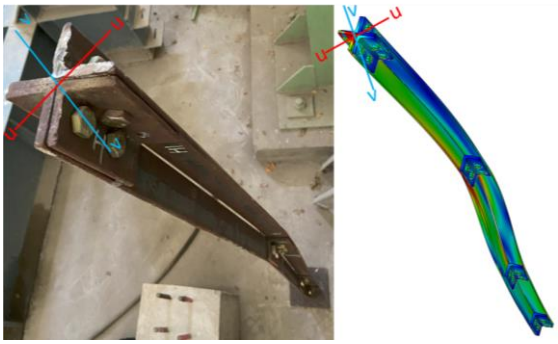

Fig. 12 Buckling axis for Bi-Angled Cruciform Specimen

Comparison of load vs lateral displacement for SR 100 and SR 120 with and without fabrication errors Fig. 14. Stiffness of SR100-BAC-Im-Num (Model with elevational difference) was similar to experimental specimen, but there is considerable difference in their load carrying capacities, showing that providing elevational difference between the EM and RM affects the ultimate capacity. For SR120 model stiffness and capacity are greater for the specimen without inclination - 97.27kN compared to 82.47kN with inclination. Fig. 15, Fig. 16 and Fig. 17 show the deformed shapes of experimental cruciform specimens along with numerical model deformed shapes obtained from numerical analysis.

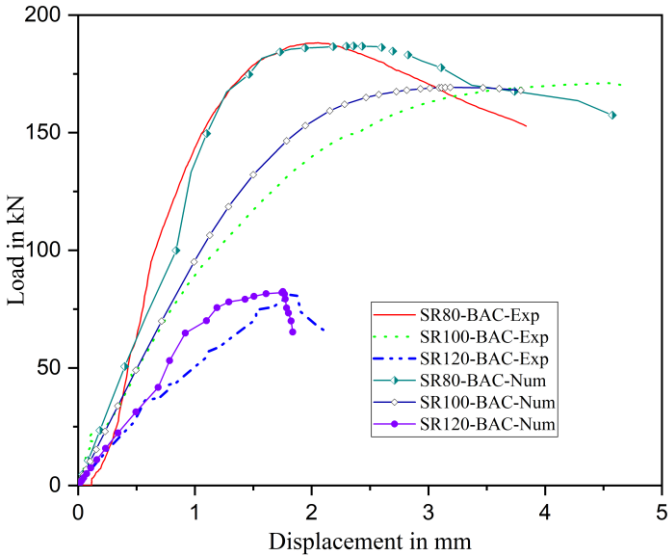

Fig. 13 Load vs Axial Displacement of Cruciform Specimens (Exp-Numerical Comparison)

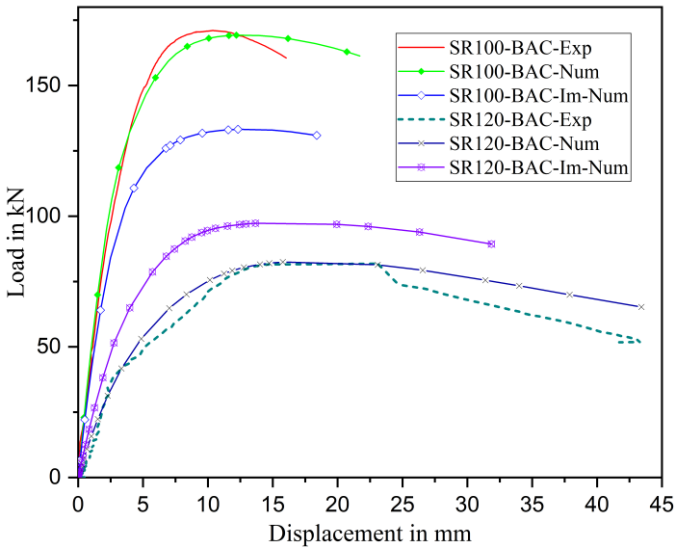

Fig. 14 Load vs Lateral Displacement for SR100 and SR120 Bi-Angles Cruciform (Comparison of models inclusive of fabrication errors)

Fig. 18 (a) to Fig. 18 (f) show the Load vs Micro Stain curves from the experiments in EM & RM for the cruciform sections and same are compared with numerical values. During the experiments, for all specimens, the highest strain at any load was recorded in the top segment of EM and least strain recorded in the top segment of RM and the same is seen in the validated numerical models. In the bottom segments of SR 80 and SR 100 specimens, the difference between the strains in EM and RM was low, indicating that the loads carried by EM and RM in the bottom segment are almost equal. In case of SR120 greater difference in strains between EM and RM compared to SR80 and SR100 were observed in the bottom segment, which may be due to higher slenderness ratio within each segment and initial inclination. In each figure, the top segment of EM which records the highest strain is the left most curve, while top segment of RM which carries least strain is the right most curve. The bottom segments of both EM and RM which carry intermediate, but similar strains, are seen in the middle of each figure. Strain in EM decreases from top segment to bottom segment, where as in RM its increases from top to bottom, which clearly depicts the load transfer through the connected angle cleats.

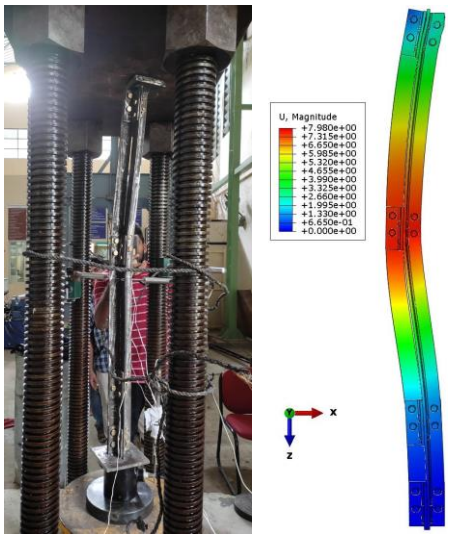

Fig. 15 SR80 Deformed Shape (Exp-Numerical)

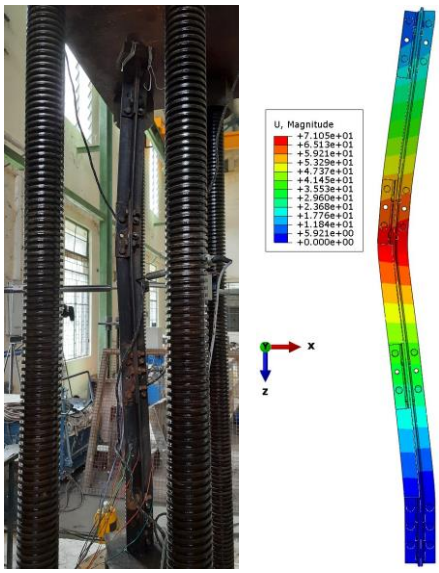

Fig. 16 SR100 Deformed Shape (Exp-Numerical)

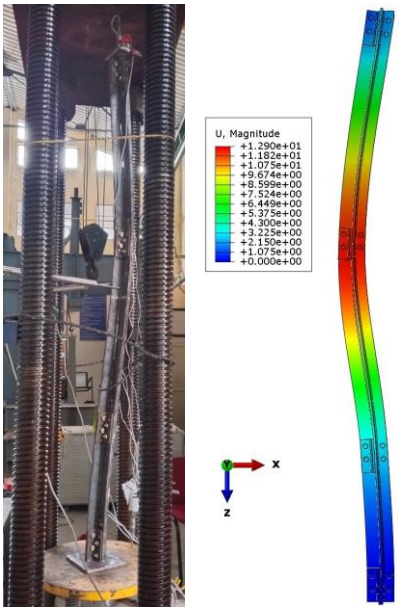

Fig. 17 SR120 Deformed Shape (Exp-Numerical)

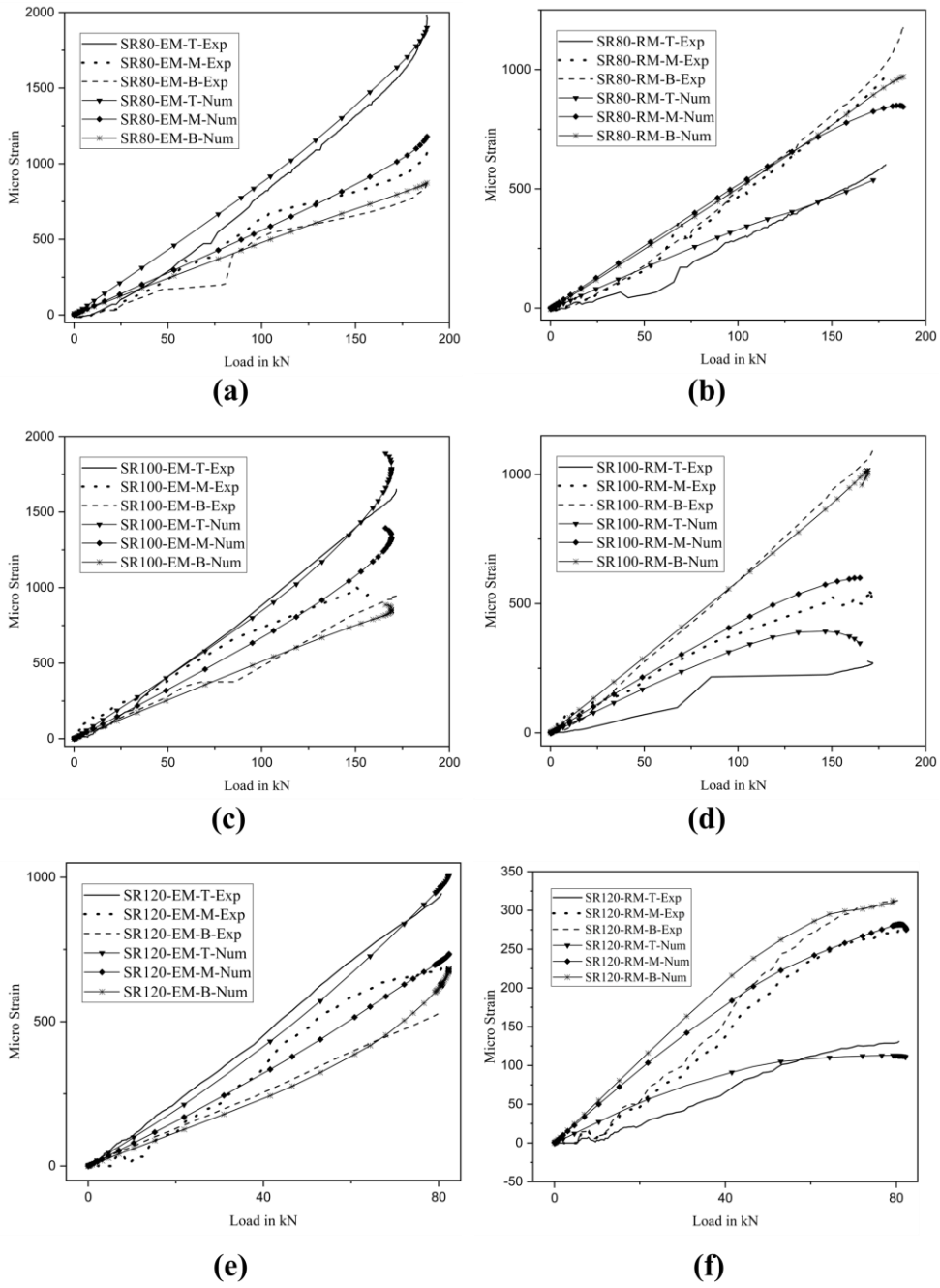

Fig. 18 Comparison of Load vs Micro Strain (T-Top; M-Middle; B-Bottom)

4.3. Codal predictions

The experimental and numerical capacities were also compared with the codal predictions. Capacity of single and bi-angled cruciform sections were calculated with the help of Indian Standard [30], European Standard[31] and AISC[26] codal provisions and compared with experimental results. From the specifications of design of compression member, the following set of equations (6-9) were used to determine the capacity by using IS:800-2007 [30] and BS EN 1993-1-1:2005 / EN 1993-1-1:2005 (E) [31]. Partial safety factors were avoided in calculations.

$$N_{b,Rd} = \chi A f_y \tag{6}$$

$$\chi = \frac{1}{\phi+[\phi^2-\lambda^2]^{0.5}} \quad but\ \chi \leq 1.0 \tag{7}$$

$$\bar{\lambda} = \sqrt{\frac{Af_y}{N_{cr}}} \tag{8}$$

$$N_{cr} = \frac{\pi^2 EI}{L_c^2} \tag{9}$$

Sections E3 & E4 of AISC: 360-16 [26] were used for determining the flexural buckling & Torsional and Flexural-Torsional buckling capacities of section respectively. The procedure available in E6 was followed to determine the modified slenderness ratio for built-up cruciforms.

$$P_n = F_{cr} A_g \tag{10}$$

Flexural Buckling Strength

$$F_{cr} = \left(0.658^{\frac{F_y}{F_e}}\right) F_y \tag{11}$$

$$F_e = \frac{\pi^2 E}{\left(\frac{L_c}{r}\right)^2} \tag{12}$$

Modified slenderness ratio for built-up section, K_i considered as 0.86.

$$\left(\frac{L_c}{r}\right)_m = \sqrt{\left(\frac{K_i a}{r_i}\right)^2 + \left(\frac{L_c}{r}\right)_o^2} \tag{13}$$

Torsional and Flexural-Torsional buckling strength

$$F_e = \left(\frac{\pi^2 EC_w}{L_{cz}^2} + GJ\right)\frac{1}{I_x + I_y} \quad (14)$$

The effective length factor (K) for the codal predictions was taken as 0.85, due to absence of degree of restraint properties for coping kind of support condition, the K value was decided based on the deformed shape of bi-angled cruciform experimental specimens. For the determination of effective slenderness ratio, radius of gyration about the minor principle axis (r_{vv}) was used since the buckling (Fig. 10 and Fig. 12) for both single and bi-angled cruciform was observed about minor principle axis.

Table 2 shows that experimental and numerical results of single angles are close to the Codal predictions of IS [30] and Euro [31] code. The capacity predicted by AISC code [26] is higher than that of the other two codes. Codal capacity (using the flexural buckling specifications with respect to IS & Euro codes) for 100 & 120 slenderness cruciform were unconservative in comparison to experimental and numerical capacity. Codal capacity (with Flexural-Torsional Buckling) in accordance with AISC specifications were in better agreement with numerical capacity for 100 & 120 slenderness specimens. Codal flexural buckling capacities obtained through IS and Euro codes are similar, since the codal expressions in both codes are identical.

Table 2
Comparison of Experimental -Numerical-Analytical Results for Experimental Specimens

S. No	Name of Model	Capacity of Section (kN)				
		Experimental	Numerical	Analytical		
				IS Code [30]	Euro [31]	AISC [26]
1	SR80-SA-Num	109.04	107	108.55 (F)	108.55 (F)	121.3 (F)
2	SR100-SA-Num	100.1	95.8	95.4 (F)	95.4 (F)	108.82 (F)
3	SR120-SA-Num	75.072	81.7	77.7 (F)	77.7 (F)	95.21 (F)
4	SR80-BAC-Num	188.237	186.87	180.1 (F)	180.15 (F)	177.55 (TF)
5	SR100-BAC-Num	171.1	169.26	-	-	-
6	SR100-BAC-Im-Num	-	133.22	145 (F)	145.03 (F)	136.46 (TF)
7	SR120-BAC-Num	81.81	82.47	-	-	-
8	SR120-BAC-Im-Num	-	97.271	111.8 (F)	111.8 (F)	97.04 (TF)

4.4. Parametric study

The parameters varied are: (a) Slenderness ratio – 80, 100 & 120; (b) Spacing of connectors – according to AISC specifications, spacing equal to (¾)L times the ratio of r_{min} of single angle to Bi-Angled cruciform section and L times the ratio of r_{min} of single angle to Bi-Angled cruciform section, where L is length of full section; (c) Number of bolts per connector – 4 & 6; (d) Width to thickness ratio (represented as Wt.R) of angle section – 6.7, 10 & 15. Fig. 19 shows, specimens with different spacing of connectors and number of bolts per connector used in the parametric study. A total of thirty-six models were thus developed and analyzed to figure out the influence of the considered parameters on capacity and load sharing rate. The list of various models along with their capacities obtained from codal predictions and numerical are mentioned in the Table 3.

Table 3
Consolidated Results for all Parametric models

S.No	Model	L (mm)	Theoretical Capacity in kN				Avg Stress in MPa	Num-Cap (kN)	Axial Stiffness (kN/mm)
			IS Code	Euro Code	AISC 360-16				
			FB	FB	FB	TFB			
1	SR80-TFS-4B-Wt.R.6.7	1200	180.1	180.2	212.9	177.6	200	186.8 (F)	122.77
2	SR80-TFS-4B-Wt.R.10	1552	191.1	191.1	226.4	190.9	215	191.2 (F)	104.93
3	SR80-TFS-4B-Wt.R.15	2368	291.7	291.6	354.5	288.6	325	274.4 (F)	96.25
4	SR80-TFS-6B-Wt.R.6.7	1200	180.1	180.2	212.9	177.6	200	190.8 (F)	124.75
5	SR80-TFS-6B-Wt.R.10	1552	191.1	191.1	226.4	190.9	215	195.6 (F)	105.68
6	SR80-TFS-6B-Wt.R.15	2368	291.7	291.6	354.5	288.6	325	290.8 (F)	105.84
7	SR80-S-4B-Wt.R.6.7	1200	180.1	180.2	212.9	154.2	173.6	172.9 (F)	119.58
8	SR80-S-4B-Wt.R.10	1552	191.1	191.1	226.4	164.8	185.6	171.5 (F)	96.8
9	SR80-S-4B-Wt.R.15	2368	291.7	291.6	354.5	248.5	279.8	264.2 (F)	93.85
10	SR80-S-6B-Wt.R.6.7	1200	180.1	180.2	212.9	154.2	173.6	176.8 (F)	121.76
11	SR80-S-6B-Wt.R.10	1552	191.1	191.1	226.4	164.8	185.6	187.7 (F)	102.91
12	SR80-S-6B-Wt.R.15	2368	291.7	291.6	354.5	248.5	279.8	271.9 (F)	101.57
13	SR100-TFS-4B-Wt.R.6.7	1500	145	145	181.3	136.5	143.7	133.2 (F)	95.61
14	SR100-TFS-4B-Wt.R.10	1940	150.2	150.7	192.1	143.7	151.3	154.1 (F)	78.41
15	SR100-TFS-4B-Wt.R.15	2960	229.9	229.7	293.1	211.2	222.3	228.9 (F)	78.01
16	SR100-TFS-6B-Wt.R.6.7	1500	145	145	181.3	136.5	143.7	144.7 (F)	98.79
17	SR100-TFS-6B-Wt.R.10	1940	150.2	150.7	192.1	143.7	151.3	166.6 (F)	81.611
18	SR100-TFS-6B-Wt.R.15	2960	229.9	229.7	293.1	211.2	222.3	240.8 (F)	82.17
19	SR100-S-4B-Wt.R.6.7	1500	145	145	181.3	106.9	112.5	123.4 (F)	92.89
20	SR100-S-4B-Wt.R.10	1940	150.2	150.7	192.1	112.6	118.5	139.8 (F)	77.19

21	SR100-S-4B-Wt.R.15	2960	229.9	229.7	293.1	169.2	178.1	211.1 (F)	76.12
22	SR100-S-6B-Wt.R.6.7	1500	145	145	181.3	106.9	112.5	137.4 (F)	96.002
23	SR100-S-6B-Wt.R.10	1940	150.2	150.7	192.1	112.6	118.5	142.4 (F)	81.02
24	SR100-S-6B-Wt.R.15	2960	229.9	229.7	293.1	169.2	178.1	217.1 (F)	81.32
25	SR120-TFS-4B-Wt.R.6.7	1800	111.8	111.9	141.7	97.04	66.9	97.2 (TF)	77.29
26	SR120-TFS-4B-Wt.R.10	2328	118.1	118.1	149.6	99.49	68.6	104.1 (TF)	62.42
27	SR120-TFS-4B-Wt.R.15	3552	180.2	180.1	228.2	144.9	99.9	161.0 (TF)	61.25
28	SR120-TFS-6B-Wt.R.6.7	1800	111.8	111.9	141.7	97.04	66.9	106.2 (TF)	81.45
29	SR120-TFS-6B-Wt.R.10	2328	118.1	118.1	149.6	99.49	68.6	109.9 (TF)	65.02
30	SR120-TFS-6B-Wt.R.15	3552	180.2	180.1	228.2	144.9	99.9	167.4 (TF)	65.74
31	SR120-S-4B-Wt.R.6.7	1800	111.8	111.9	141.7	68.57	47.3	96.0 (TF)	76.73
32	SR120-S-4B-Wt.R.10	2328	118.1	118.1	149.6	70.9	48.9	96.7 (TF)	61.33
33	SR120-S-4B-Wt.R.15	3552	180.2	180.1	228.2	106.4	73.4	152.1 (TF)	59.93
34	SR120-S-6B-Wt.R.6.7	1800	111.8	111.9	141.7	68.57	47.3	100.6 (TF)	79.221
35	SR120-S-6B-Wt.R.10	2328	118.1	118.1	149.6	70.9	48.9	100.9 (TF)	64.25
36	SR120-S-6B-Wt.R.15	3552	180.2	180.1	228.2	106.4	73.4	156.2 (TF)	64.89

Wt.R - Width/Thickness Ratio; for Wt.R 6.7 ISA40X40X6, Wt.R 10 ISA 50X50X5, Wt.R 15 ISA 75X75X5 were used; TFS - (3/4)*Spacing & S - Spacing (S); 4B - 4 Bolts per each cleat angle, 6B - 6 Bolts per each cleat angle; L – Length of the model; C/C-C – Centre to Centre of connectors.

From Fig. 20 (a) to Fig. 20 (c) it is seen that the load vs lateral displacement behavior varies with spacing of connectors as well as the number of bolts per connector. For any slenderness ratio and width to thickness ratio of 6.7, sections with TFS (3/4 spacing) and six bolts per connector takes highest load due to low slenderness ratio of each segment and longer load transfer path. The effect of width to thickness ratio is depicted in Fig. 20 (d) which shows the stress vs lateral displacement for the SR80 specimen with TFS (3/4 spacing) and four bolts per connector at various width to thickness ratios. It clearly seen that the stiffness of model decreases with the increase in the width to thickness ratio since stiffness of individual angle leg tends to reduce with increasing width to thickness ratio, leading to reduction in the overall stiffness of the section.

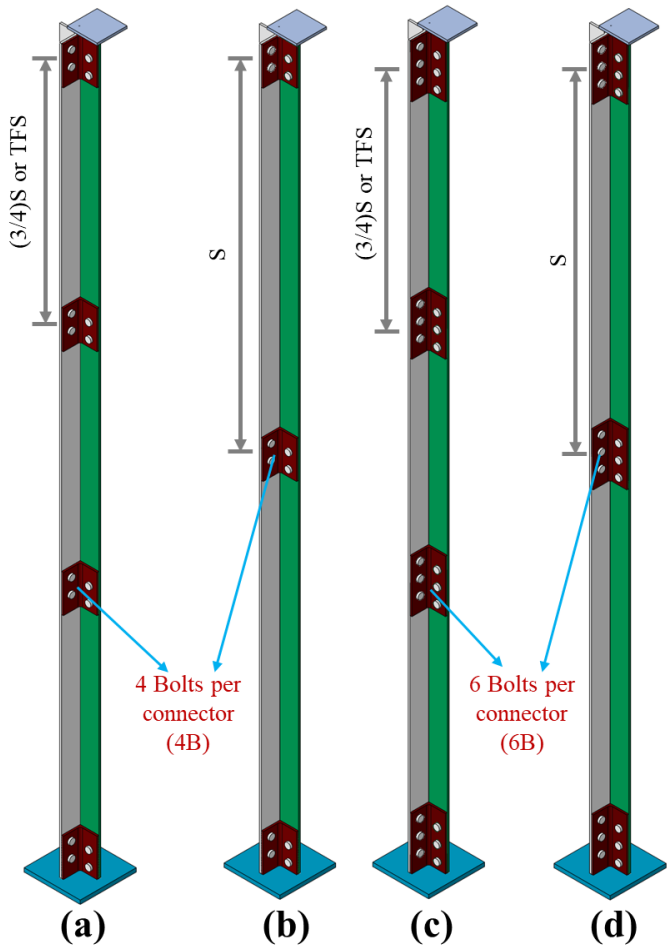

Fig. 19 (a) Various Cruciform sections in parametric study; (a) (¾)S with 4 bolts per connector, (b) "S" with 4 bolts per connector, (c) (¾)S with 6 bolts per connector, (d) "S" with 6 bolts per connector

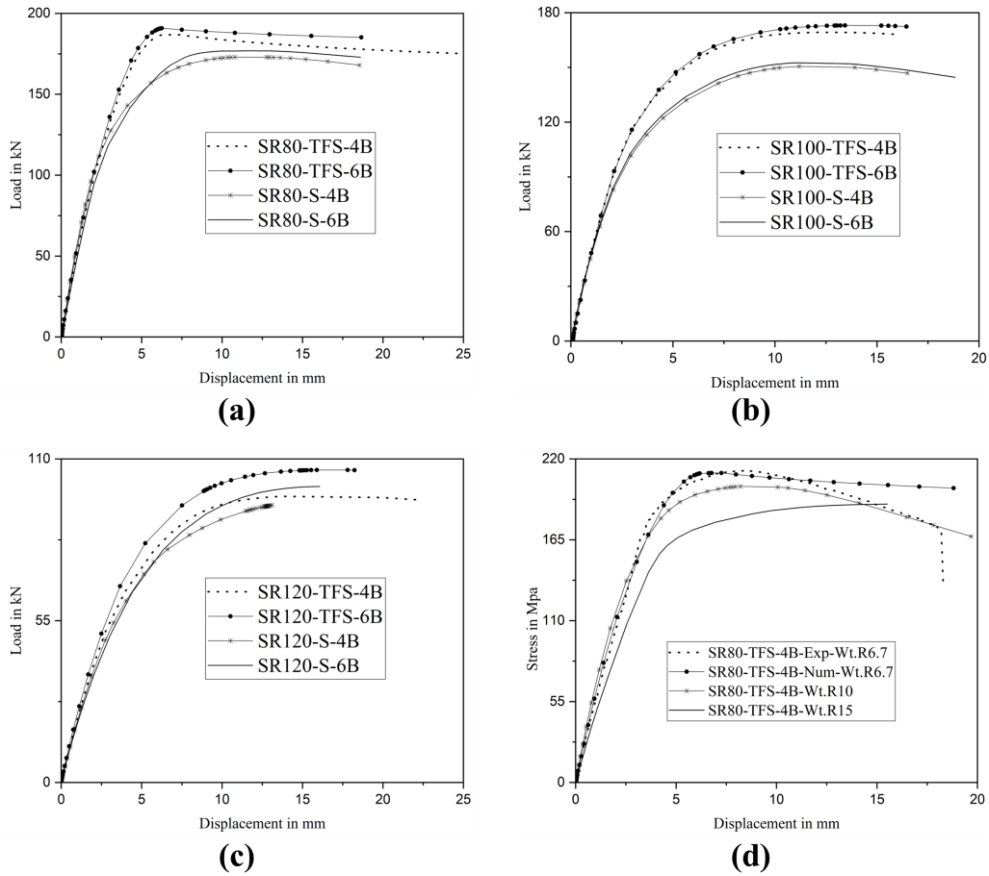

Fig. 20 (a) Load vs Lateral Displacement for 80 Slender and width to thickness ratio of 6.7; (b) Load vs Lateral Displacement for 100 Slender and width to thickness ratio of 6.7; (c) Load vs Lateral Displacement for 120 Slender and Wt.R6.7; (d) Stress vs Lateral Displacement for SR80 with various width to thickness ratios

Table 3 also shows the axial stiffness (kN/mm) for all parametric study models. For specimens of same slenderness, compared to other parameters, it was noticed from the results that the axial stiffness is highly influenced by variation in width to thickness ratio. As an example, for SR80-TFS-4B model and width to thickness ratio of 6.7, stiffness is 122.77 kN/mm whereas it reduces to 104.93 kN/mm and 96.25 kN/mm for width to thickness ratio of 10 and width to thickness ratio of 15 respectively. There is slight reduction in the stiffness observed for any model when spacing of connectors increased from TFS (¾ S) to S, and slight increase in stiffness when number bolted increased from 4 to 6. Axial stiffness of models with TFS-4B-Wt.R6.7 reduces from 122.77 kN/mm for SR80 to 95.61 kN/mm for SR100 and its further reduces to 77.29 for SR120, showing that slenderness ratio influences the axial stiffness considerably.

4.5. Load sharing rate

One of the major objectives of study was to investigate the load transferring mechanism from the Existing Member (EM) to Reinforcing Member (RM) through the cleat angles. The stress transmission from EM to RM is clearly observed from Fig. 21 in the axial direction for all cruciform specimens. All figures show EM on the right hand side and RM on the left hand side. It is clearly visible that stress in EM reduces from top to bottom, whereas for RM it increases. It is observed that the high stress which is present in the top segment of EM (Fig. 21) reduces with increase in the slenderness ratio, which is due to reduction in the capacity of the specimen with increase in slenderness ratio. The three rows in Fig. 22 show the cross-sectional stress variation among the EM and RM at mid-height of each segment for SR 80, SR 100 and SR 120 for width to thickness ratio of 6.7.

Field output values by probing S33 (in axial direction) was extracted for every element at the mid height cross section of each segment and then multiplied by the element cross-sectional area which provides the total load at the cross-section in a particular member (EM or RM). As an example, for 80SR-TFS-4B-Wt6.7, the load sharing details are mentioned in Table 4. The load sharing at the bottom segment is of utmost interest for practical purpose, hence Table 5, Table 6 and Table 7 show the consolidated load sharing only at the bottom segment of all specimens of 80SR, 100SR and 120SR respectively.

4.5.1. Effect of connector spacing on load sharing

From Fig. 23 it is clear that, for models with same slenderness ratio and number of bolts per connector, there is a reduction in percentage of load transferring from EM to RM in models with connector spacing of S when compared with TFS (3/4 Spacing). Percentage reduction of load sharing for models with spacing S varies from an average of 19.9% to a maximum of 29.9%. The individual segments slenderness ratio is high in the models with spacing S, when compared with the models with TFS, which is the plausible reason for less load transferring in models with spacing S.

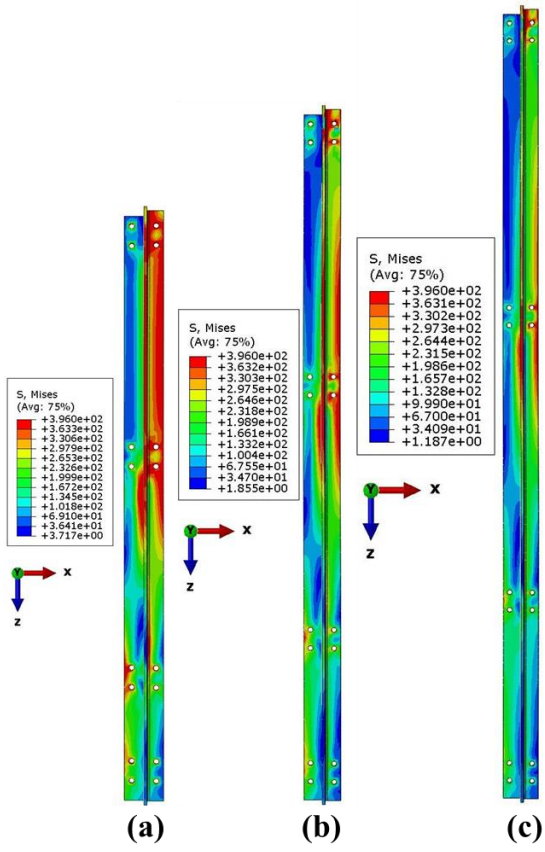

Fig. 21 Variation of Stresses in the EM & RM in longitudinal direction (a) SR80; (b) SR100; (c) SR120

4.5.2. Effect of bolts per connector on load sharing

There is a considerable influence of the number of bolts per connector in the load sharing between the EM and RM. This can be observed in Fig. 23 by comparing any two bar columns with different bolts per connector and all other parameters same. There is an average increase of 19.29% to maximum of 35.7% of load sharing happens in models with 6B (six bolts per connector) than compared to models with 4B (four bolts per connector). The cumulative intensity of bolt pre-tension force is more in models with 6B, which establishes a greater bearing resistance between the EM and RM than models with 4B, which may lead to higher load sharing for 6B models.

4.5.3. Effect of slenderness ratio on load sharing

It is clear from Fig. 23 that for any combination of parameters with increase in slenderness ratio load sharing reduces. Average of 6.52% to a maximum of 12.8% reduction in load sharing for 100 slenderness specimens observed compared to 80 slender specimens. It is about 28.2% average to 35.06% maximum for 120 slenderness compared to 100 slenderness specimens. SR120 specimen's flexural torsional type of failure which differs from failure mode of SR80 and SR100 (Flexural mode) causes the lower load sharing rate. In addition, segmental slenderness ratio for SR120 specimen is higher than in other two specimens.

Table 4
Load Sharing of 80SR-TFS-4B-Wt6.7 (80SR Exp)

Location @mm	Load		Percentage of Load in RM
	Existing Member (EM)	Reinforcing Member (RM)	
Top of EM	185.33		
Top Segment @ 305	142.86	43.52	23.35%
Middle Segment @755	122.06	65.08	34.78%
Bottom Segment @1055	83.43	102.03	55.02%

Table 5
Load Sharing between the EM & RM at Mid height of last segment for 80SR specimens

S. No	Model	Total Capacity in kN	Load Sharing in kN		Percentage of Load in RM
			Existing Member (EM)	Reinforcing Member (RM)	
1	80SR-TFS-4B- Wt.R.6.7	186.87	83.43	102.03	54.60%
2	80SR-TFS-6B-Wt.R.6.7	190.89	76.56	114.14	59.90%
3	80SR-S-4B-Wt.R.6.7	172.93	99.13	73.61	42.57%
4	80SR-S-6B-Wt.R.6.7	176.869	92.75	83.40	47.15%
5	80SR-TFS-4B-Wt.R.10	191.23	99.67	91.19	47.68%
6	80SR-TFS-6B-Wt.R.10	195.648	94.79	98.70	50.45%
7	80SR-S-4B-Wt.R.10	171.55	113.38	60.52	35.28%
8	80SR-S-6B-Wt.R.10	187.74	108.90	80.92	43.10%
9	80SR-TFS-4B-Wt.R.15	274.478	167.00	107.72	39.25%
10	80SR-TFS-6B-Wt.R.15	290.852	153.07	136.91	47.07%
11	80SR-S-4B-Wt.R.15	264.242	188.32	73.33	28.97%
12	80SR-S-6B-Wt.R.15	271.954	168.59	102.43	37.66%

Table 6
Load Sharing between the EM & RM at Mid height of last segment for 100SR specimens

S. No	Model	Total Capacity in kN	Load Sharing in kN		Percentage of Load in RM
			Existing Member (EM)	Reinforcing Member (RM)	
1	SR100-TFS-4B-Wt.R.6.7	133.22	67.46	67.70	50.82%
2	SR100-TFS-6B-Wt.R.6.7	144.78	61.53	82.90	57.40%
3	SR100-S-4B-Wt.R.6.7	123.45	74.46	47.35	38.36%
4	SR100-S-6B-Wt.R.6.7	137.415	74.57	64.01	46.58%
5	100SR-TFS-4B-Wt.R.10	154.197	84.07	68.76	44.59%
6	100SR-TFS-6B-Wt.R.10	166.695	87.55	77.96	46.77%
7	100SR-S-4B-Wt.R.10	139.83	91.73	47.23	33.78%
8	100SR-S-6B-Wt.R.10	142.483	84.78	56.41	39.59%
9	100SR-TFS-4B-Wt.R.15	228.616	142.61	83.67	36.60%
10	100SR-TFS-6B-Wt.R.15	240.884	133.70	106.54	44.23%
11	100SR-S-4B-Wt.R.15	211.164	149.24	61.18	27.75%
12	100SR-S-6B-Wt.R.15	217.104	145.38	71.30	32.84%

4.5.4. Effect of width to thickness ratio on load sharing:

From the results, it is found that for any slenderness ratio there is considerable reduction in the load sharing rate with increase in the width to thickness ratio of the angle legs. For example in case of SR80 with TFS spacing and 4B connectors for Wt.R 6.7 the load sharing rate is 55.02% where for the Wt.R 15 load sharing is 39.12%. From Fig. 23 for any set of other constant parameters

with increase in width to thickness ratio from 6.7 to 10, it was observed that average of 14.45% to maximum of 22.31% reduction in load sharing happened. Similarly, for width to thickness ratio of 10 to 15 there is 14.06% average to 21.34% reduction in load sharing can be seen.

Table 7
Load Sharing between the EM & RM at Mid height of last segment for 120SR specimens

S. No	Model	Total Capacity in kN	Load Sharing in kN		Percentage of Load in RM
			Existing Member (EM)	Reinforcing Member (RM)	
1	120SR-TFS-4B-Wt.R 6.7	97.271	63.20	33.84	34.79%
2	120SR-TFS-6B-Wt.R.6.7	106.247	63.20	44.25	41.65%
3	120SR-S-4B-Wt.R.6.7	96.053	70.25	26.74	27.84%
4	120SR-S-6B-Wt.R.6.7	100.644	64.37	33.89	33.67%
5	120SR-TFS-4B-Wt.R.10	104.124	73.23	30.15	28.96%
6	120SR-TFS-6B-Wt.R.10	109.995	69.84	39.24	35.67%
7	120SR-S-4B-Wt.R.10	96.724	75.75	22.09	22.84%
8	120SR-S-6B-Wt.R.10	100.922	68.87	30.98	30.69%
9	120SR-TFS-4B-Wt.R.15	161.034	121.43	38.64	23.99%
10	120SR-TFS-6B-Wt.R.15	167.419	118.56	48.43	28.93%
11	120SR-S-4B-Wt.R.15	152.144	119.93	32.04	21.06%
12	120SR-S-6B-Wt.R.15	156.259	107.00	42.27	27.05%

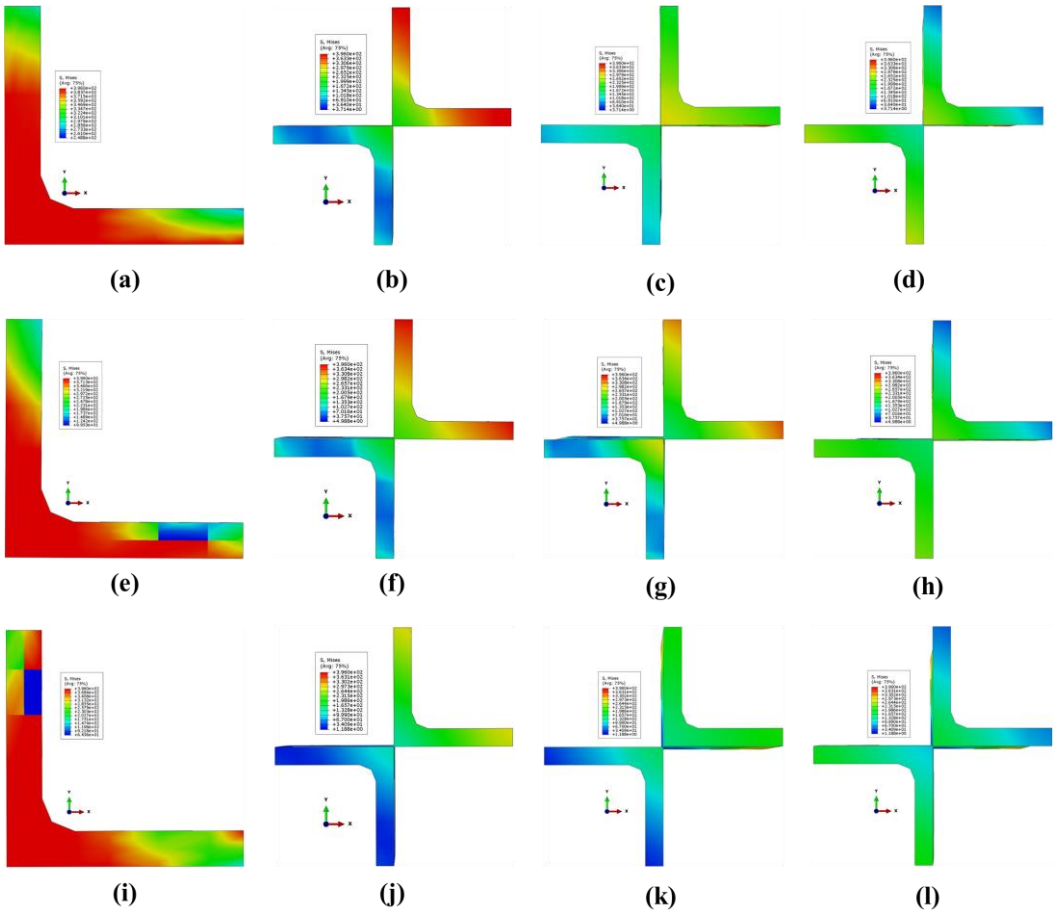

Fig. 22 Stress distribution in between EM & RM at various cross – sections top to bottom (left to right) for Wt.R.6.7; (a) to (d) – SR80-TFS-4B; (e) to (h) – SR100-TFS-4B; (i) to (l) – SR120-TFS-4B

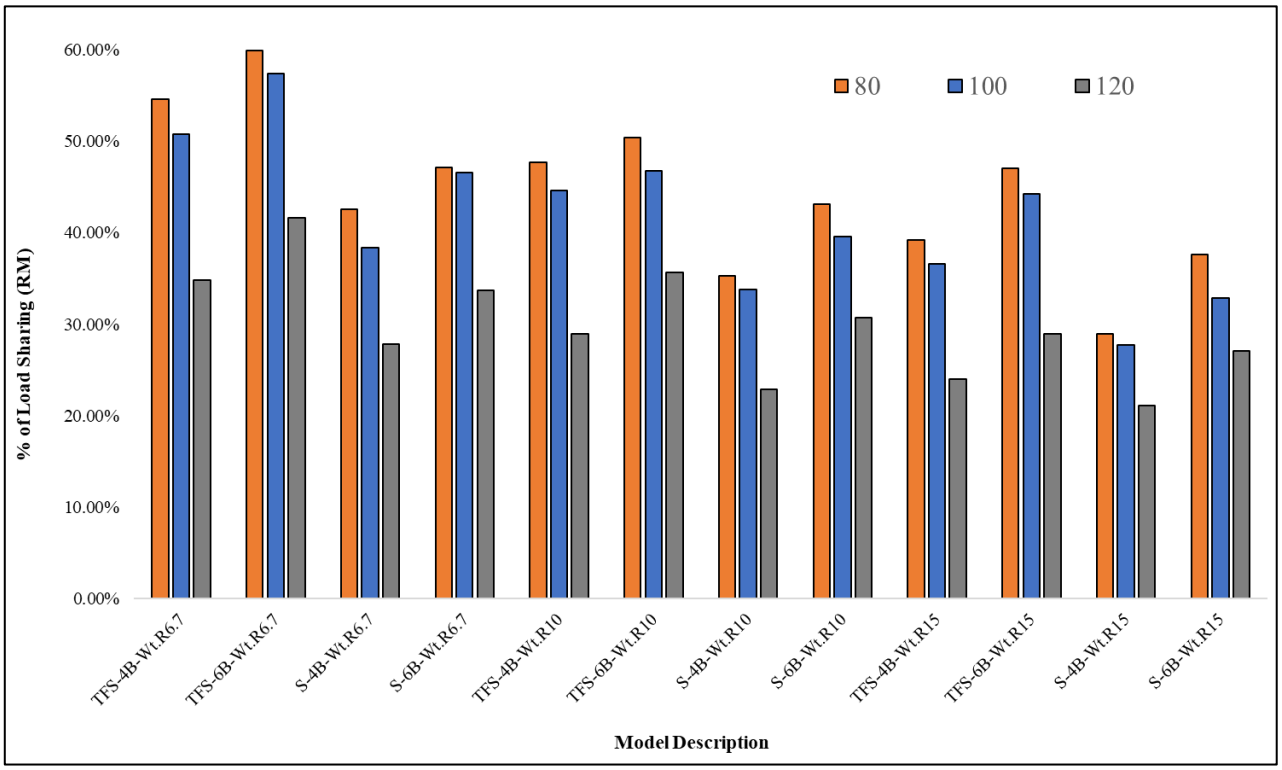

Fig. 23 Variation of Percentage of Load Carrying by RM with Various Slenderness Ratio

5. Conclusions

In the present study, the behavior of Bi-Angled Cruciform (BAC) sections made by connecting two angle sections vertex to vertex were tested for three different slenderness ratio (80, 100 and 120) under compression through one angle. Numerical models developed in ABAQUS were validated with the experimental results followed by a parametric study with 36 models to investigate the effect of various parameters, namely, slenderness ratio, spacing of connectors, number of bolts per connector and width to thickness ratio. The experimental and numerical capacities were also compared with codal predictions using Indian Standard, Euro Code and AISC specifications. The load sharing between the EM and RM is the key result to show the application of the retrofit arrangement. The following conclusions can be drawn:

i. These bi-angled cruciform provide 20% to 83% increase in capacity as single angles of same slenderness as against 100% increase expected theoretically. The increase percentage decreases with overall specimen slenderness. However, this increase in capacity shows that the cruciform arrangement is capable as a quick in-situ solution for intervention.

ii. The experiment (SR100-BAC) where the top loading plate attained contact with RM shows that there is a significant difference in capacity (21%) in comparison with cruciform loaded through the centroid of EM which transfer loads via the connectors to RM. This difference is not significant at lower slenderness (SR80).

iii. All models of SR80 and SR100 failed by flexural buckling while SR120 models fail in flexural-torsional mode. Consequently, IS and Euro code prediction were close to the numerically obtained values when using flexural buckling equation. The AISC code which contains a slenderness factor (K_i) for built-up sections over predicts the flexural buckling capacity.

iv. From the diagrams, the transfer of load from EM to RM is shown to be more efficient in cruciform arrangement for lower slenderness. For higher slenderness, improvements can be obtained with more fasteners per connection and/or lower inter-connection spacing. The load-sharing rate ranges from 20% in the top segments to up to 50% at the bottom most segments highlighting the importance of the connection arrangements in achieving the required load sharing.

v. From the conducted parametric study results, the influence of parameters can be ranked in descending order as follows: overall slenderness, angle leg width to thickness ratio, spacing of connectors and lastly, bolts per connector. On overall load sharing in SR120 specimens is only 35%, and width to thickness ratio 15 leads to sharing rate as low as 22%. Therefore, these parameters can be chosen carefully to achieve efficient load transfer in the built-up cruciform for the retrofit.

vi. The ideal load sharing rate in any retrofitting technique is 50% each in Existing Member (EM) and Reinforcing Member (RM). From the results it is seen that this is achieved only at lower slenderness ratio (80) and low width to thickness ratio (6.7) and when employing TFS-spacing for connectors. The load share in the RM falls below 50% at the same slenderness ratio when the connector spacing is S. For the two higher slenderness ratios (100 and 120) the load share in RM does not reach 50% for any case, even though in all cases the TFS-spacing resulted in the higher load share in RM. Therefore AISC 360-16 [26] recommendation pertaining to maximum connector spacing shall be followed in order to achieve the maximum possible load share in RM, though this will not always result in 50% load share.

Consideration of the preload in Existing Member (EM) before addition of the Reinforcing Member (RM) and influence of the preload on the overall built-up section can be taken as future scope of research.

Nomenclature

SA	Single Angle	f_y	Characteristic yield stress (IS 800)
BAC	Bi-Angled Cruciform section	λ	non-dimensional effective slenderness ratio (IS 800)
SR 80	Slenderness Ratio of 80, Similarly for SR100 and SR 120	α	Imperfection factor (IS 800 & EN 1993-1-1:2005)
TFS	Center to center connector spacing equal to "(¾)*L times the ratio of r_{min} of single angle to Bi-Angled cruciform section"	N_b, R_d	Design buckling resistance of compression member (EN 1993-1-1:2005)
S	Center to center connector spacing equal to "L times the ratio of r_{min} of single angle to Bi-Angled cruciform section"	χ	Reduction factor (EN 1993-1-1:2005)

4B	4 Bolts per one angle cleat	$\bar{\lambda}$	Non-dimensional slenderness (EN 1993-1-1:2005)
6B	6 Bolts per one angle cleat	N_{cr}	Elastic critical force (EN 1993-1-1:2005)
Wt.R 6.7	Width to thickness ratio of 6.7 for angle, similarly Wt.R 10 and Wt.R 16	L_c	Effective Length (EN 1993-1-1:2005)
A	Cross-sectional area of SA or BAC	I	Moment of Inertia (EN 1993-1-1:2005)
I_x/I_y	Moment of Inertia about x-x axis/y-y axis	P_n	Nominal axial strength (AISC 360-16)
I_{xy}	Product of Inertia	F_{cr}	Critical stress (AISC 360-16)
I_{min}	Minimum moment of Inertia	A_g	Gross area of member (AISC 360-16)
r_{min}	Minimum radius of gyration	F_y	Specified minimum yield stress (AISC 360-16)
SR	Slenderness Ratio	F_e	Elastic buckling stress (AISC 360-16)
L	Length of SA/BAC specimens	$(Lc/r)_m$	Modified slenderness ratio for built-up section (AISC 360-16)
P_d	Design compressive strength (IS 800)	C_w	Warping Constant (AISC 360-16)
A_e	effective sectional area (IS 800)	L_{cz}	Effective length of member for buckling about longitudinal axis (AISC 360-16)
f_{cd}	Design compressive stress (IS 800)		

References

[1] A. H. A. Abdelrahman, Z.-L. Du, Y.-P. Liu, and S.-L. Chan, "Stability design of single angle member using effective stress-strain method," Structures, vol. 20, pp. 298–308, Aug. 2019, doi: 10.1016/j.istruc.2019.04.013.

[2] W.-Q. Jiang, Y.-P. Liu, S.-L. Chan, and Z.-Q. Wang, "Direct Analysis of an Ultrahigh-Voltage Lattice Transmission Tower Considering Joint Effects," Journal of Structural Engineering, vol. 143, no. 5, May 2017, doi: 10.1061/(ASCE)ST.1943-541X.0001736.

[3] A. Hussain, Y.-P. Liu, and S.-L. Chan, "Finite Element Modeling and Design of Single Angle Member Under Bi-axial Bending," Structures, vol. 16, pp. 373–389, Nov. 2018, doi: 10.1016/j.istruc.2018.11.001.

[4] E. Murtha-Smith and H. R. Adibjahromi, "Restrained Warping in Cruciform Compression Members," Journal of Structural Engineering, vol. 114, no. 1, pp. 198–210, Jan. 1988, doi: 10.1061/(ASCE)0733-9445(1988)114:1(198).

[5] M. C. Temple, S. S. S. Sakla, D. Stchyrba, and D. Ellis, "Arrangement of interconnectors for starred angle compression members," Canadian journal of civil engineering, vol. 21, no. 1, 1994, doi: 10.1139/l94-007.

[6] I. S. Botelho et al., "Starred rolled stainless steel angle sections under compression: An experimental and numerical investigation," Thin-Walled Structures, vol. 158, Jan. 2021, doi: 10.1016/j.tws.2020.107177.

[7] J. ke Han, C. lei Zhang, Z. bao Li, and X. ming Wang, "Stability analysis of closely star-battened member of transmission tower," International Journal of Steel Structures, vol. 17, no. 3, pp. 949–956, Sep. 2017, doi: 10.1007/s13296-017-9007-8.

[8] B. Li, P. Cao, D. Zhang, and Y. Guo, "Experimental research on behavior of Q420 dual-angle steel with cruciform section under dynamic compression," Journal of Vibroengineering, vol. 19, no. 3, pp. 2031–2042, 2017, doi: 10.21595/jve.2016.17794.

[9] R. Balagopal, N. Prasad Rao, R. P. Rokade, and P. K. Umesha, "Studies on strengthening techniques for existing transmission line and communication towers," in Lecture Notes in Civil Engineering, vol. 12, Springer, 2019, pp. 639–648. doi: 10.1007/978-981-13-0365-4_54.

[10] N. Ungkurapinan, S. R. D. S. Chandrakeerthy, R. K. N. D. Rajapakse, and S. B. Yue, "Joint slip in steel electric transmission towers," Eng Struct, vol. 25, no. 6, pp. 779–788, 2003, doi: 10.1016/S0141-0296(03)00003-8.

[11] E. Baran, T. Akis, G. Sen, and A. Draisawi, "Experimental and numerical analysis of a bolted connection in steel transmission towers," J Constr Steel Res, vol. 121, pp. 253–260, Jun. 2016, doi: 10.1016/j.jcsr.2016.02.009.

[12] C. Lu, X. Ma, and J. E. Mills, "The structural effect of bolted splices on retrofitted transmission tower angle members," J Constr Steel Res, vol. 95, pp. 263–278, Apr. 2014, doi: 10.1016/j.jcsr.2013.12.011.

[13] F. Albermani, M. Mahendran, and S. Kitipornchai, "Upgrading of transmission towers using a diaphragm bracing system," Eng Struct, vol. 26, no. 6, pp. 735–744, May 2004, doi: 10.1016/j.engstruct.2004.01.004.

[14] Q. Xie and L. Sun, "Failure mechanism and retrofitting strategy of transmission tower structures under ice load," J Constr Steel Res, vol. 74, 2012, doi: 10.1016/j.jcsr.2012.02.003.

[15] Y. Zhuge, J. E. Mills, and X. Ma, "Modelling of steel lattice tower angle legs reinforced for increased load capacity," Eng Struct, vol. 43, pp. 160–168, Oct. 2012, doi: 10.1016/j.engstruct.2012.05.017.

[16] J. E. Mills, X. Ma, and Y. Zhuge, "Experimental study on multi-panel retrofitted steel transmission towers," J Constr Steel Res, vol. 78, pp. 58–67, Nov. 2012, doi: 10.1016/j.jcsr.2012.06.004.

[17] V. K. Shukla, M. Selvaraj, and K. V. Kumar, "Failure Analysis of a Cruciform-Leg Transmission Line Tower," International Journal of Steel Structures, vol. 21, no. 2, pp. 539–548, Apr. 2021, doi: 10.1007/s13296-021-00454-5.

[18] C. Lu, X. Ma, and J. E. Mills, "Modeling of retrofitted steel transmission towers," J Constr Steel Res, vol. 112, pp. 138–154, Sep. 2015, doi: 10.1016/j.jcsr.2015.04.005.

[19] L. Sun, M. Trovato, and B. Stojadinović, "In-situ retrofit strategy for transmission tower structure members using light-weight steel casings," Eng Struct, vol. 206, 2020, doi: 10.1016/j.engstruct.2020.110171.

[20] X. Guo, S. Zong, Z. Shen, S. Zhu, and S. Yuan, "Mechanical behavior of in-service axial compression angle steel members strengthened by welding," Journal of Building Engineering, vol. 32, Nov. 2020, doi: 10.1016/j.jobe.2020.101736.

[21] B. Mou, Y. Zhou, Q. Qiao, and J. Liu, "Compressive behavior of bolted built-up steel columns fabricated using angle section columns," Journal of Building Engineering, vol. 44, Dec. 2021, doi: 10.1016/j.jobe.2021.103260.

[22] G. Liang, L. Wang, Y. Liu, and N. Geng, "Mechanical behavior of steel transmission tower legs reinforced with innovative clamp under eccentric compression," Eng Struct, vol. 258, May 2022, doi: 10.1016/j.engstruct.2022.114101.

[23] Q. Xie and J. Zhang, "Experimental study on failure modes and retrofitting method of latticed transmission tower," Eng Struct, vol. 226, 2021, doi: 10.1016/j.engstruct.2020.111365.

[24] A. M. Taha, M. A. Dabaon, M. H. El-Boghdadi, and M. F. Hassanein, "Experimental testing and evaluation of real-scale lap-splice bolted connections used in typical lattice steel transmission towers," Thin-Walled Structures, vol. 171, Feb. 2022, doi: 10.1016/j.tws.2021.108790.

[25] "Indian Standard USE OF STRUCTURAL STEEL IN OVERHEAD TRANSMISSION LINE TOWERS-CODE OF PRACTICE IPJSRT 1 MATERIALS, LOADS AND PERMISSIBLE STRESSES Section 1 Materials and Loads," 1995.

[26] "Specification for Structural Steel Buildings," 2016.

[27] John H. Bickford, Introduction to the Design and Behavior of Bolted Joints, 4th ed. CRC Press, Taylor & Francis group, 2008.

[28] "Designation: E8/E8M − 13a Standard Test Methods for Tension Testing of Metallic Materials 1," 2019, doi: 10.1520/E0008_E0008M-13A.

[29] A. H. A. Abdelrahman, Y.-P. Liu, and S.-L. Chan, "Advanced joint slip model for single-angle bolted connections considering various effects," Advances in Structural Engineering, vol. 23, no. 10, pp. 2121–2135, Jul. 2020, doi: 10.1177/1369433220906226.

[30] B. of Indian Standards, "IS 800 (2007): General Construction In Steel - Code of Practice."

[31] "EN 1993-1-1: Eurocode 3: Design of steel structures - Part 1-1: General rules and rules for buildings."